Discover Oncology

RESEARCH Open Access

# Multi-Omics reveals SPP1 + malignant and CXCR4$^+$ TAM crosstalk predicts immunotherapy response in lung adenocarcinoma

Bei li Wang[1], Juan wen Lian[1], Jia ling Xu[1], Tao Hua[1], Jie Ding[1], Tuo Wang[1], Cong Cao[1] and Ze jie Liu[1*]

*Correspondence:
Ze jie Liu
17791416383@163.com
[1]Xi 'an Chest Hospital, Xi 'an 710010, Shaanxi, China

## Abstract

**Background** Lung adenocarcinoma (LUAD), a common lung cancer subtype, is significantly influenced by the immune microenvironment. Immune checkpoint inhibitors have shown limited efficacy in Lung adenocarcinoma due to the immunosuppressive tumor microenvironment (TME). Identifying predictive biomarkers for immunotherapy response remains an urgent clinical need.

**Methods** Multi-Omics data of LUAD were analyzed to investigate the immune microenvironment in LUAD. Single cell RNA-seq was used for exploring the intercellular communication mechanisms in TME. Spatial transcriptomic analysis confirmed the spatial co-localization of SPP1$^+$ Malignant and CXCR4$^+$ TAM, while in vitro experiments validated the functions of biomarker.

**Results** This study delineated the cellular heterogeneity and dynamic shifts within the LUAD tumor microenvironment, resolving the malignant transformation trajectory. Crucially, we identified SPP1$^+$ malignant and CXCR4$^+$ TAM crosstalk as a driver of exhaustion of CD8T, which induced poor immunotherapy response. Moreover, this study indicated that the immune escape potential of patients in high infiltration of SPP1$^+$ malignant and CXCR4$^+$ TAM increased, and the efficacy of immune checkpoint suppressive therapy might be poorer. Spatial transcriptomics confirmed co-localization of SPP1$^+$ Malignant and CXCR4$^+$ TAM, while in vitro experiments demonstrated that CXCR4 plays an important role in the functions of LUAD cells.

**Conclusions** This study uncovers the SPP1$^+$ malignant and CXCR4$^+$ TAM crosstalk as a novel TME-driven resistance mechanism and provides a potential biomarker for stratifying LUAD patients likely to benefit from immunotherapy.

**Keywords** Tumor-associated macrophages, Prognosis, Immune microenvironment, Immunotherapy, Biomarker

## 1 Introduction

Lung cancer is responsible for a disproportionately high percentage of cancer-related mortalities globally, presenting a significant threat to public health [1]. Among its various subtypes, lung adenocarcinoma (LUAD) has emerged as the most prevalent form, currently constituting around 50% of all lung cancer diagnoses [2]. Despite its high incidence, the prognosis for LUAD patients remains dismal, with a 5-year survival rate hovering at approximately 15% [3, 4]. Building on our understanding of the tumor immune microenvironment (TIME), these insights are now translating into life-saving therapies. This progress is urgently needed given the grim reality of lung cancer, which demands a deeper investigation into its pathogenesis and the development of early diagnostic and treatment strategies. Such efforts are crucial for improving clinical outcomes. For patients with inoperable lung adenocarcinoma (LUAD), molecular targeted therapy and immunotherapy have brought new hope. Immune checkpoint inhibitors, such as nivolumab and pembrolizumab, exemplify this progress by blocking CTLA-4 and PD-1/PD-L1 signaling. This action revitalizes the TIME, enabling immune cells to effectively target and destroy tumors [5–7]. In contrast, studies have found that overexpression or supplementation of CXCR4 can also inhibit tumor progression [8]. However, similar to traditional targeted therapy, only a portion of patients can benefit from it. Therefore, seeking reliable biomarkers that can accurately predict the efficacy and prognosis of anti-PD-1 immunotherapy is crucial for achieving individualized diagnosis and treatment of LUAD.

The tumor immune microenvironment (TIME) is a critical regulator of tumorigenesis, progression, and therapeutic response. It is a dynamic ecosystem composed of immune cells, stromal cells, and the extracellular matrix, which collectively orchestrate antitumor immunity through intricate cell-cell interactions and cytokine signaling [9–12]. The relationship between tumor cells and immune cells is particularly complex and dynamic [13]. While immune cells can recognize and eliminate malignant cells, they are often co-opted by the tumor to establish an immunosuppressive niche that facilitates disease progression [14].

Notably, inflammation plays a pivotal role in the relationship between the immune microenvironment and LUAD [10, 15, 16]. Inflammatory response is a defense mechanism of the body against stimuli, but long-term chronic inflammation is closely associated with the occurrence and development of tumors [17, 18]. In LUAD, the infiltration of inflammatory cells and the release of inflammatory mediators can alter the balance of the immune microenvironment, promoting the proliferation, survival, and metastasis of tumor cells [18, 19]. For instance, cytokines secreted by inflammatory cells, such as interleukin-6 (IL-6) and tumor necrosis factor-α (TNF-α), can activate oncogenic signaling pathways in tumor cells, enhancing their invasive and metastatic capabilities [20–22].

Tumor-associated macrophages (TAMs) constitute a major component of the tumor immune microenvironment and serve as pivotal mediators of tumor-promoting inflammation [23,24]. These cells are recruited by tumor cells and undergo polarization toward an immunosuppressive phenotype. Within the inflammatory tumor microenvironment, TAMs facilitate tumor growth, proliferation, invasion, and metastasis through the secretion of various cytokines. Notably, they produce vascular endothelial growth factor (VEGF) to stimulate angiogenesis and release immunosuppressive factors such as

interleukin-10 (IL-10), which dampens the host anti-tumor immune response [24]. For example, TAM-derived VEGF promotes the formation of new blood vessels, providing nutrients and oxygen for tumor cells and facilitating their dissemination [25]. Understanding the detailed mechanism of TAM action, especially its regulatory role in the context of inflammation, holds great promise for developing novel cancer therapies [26].

The C-X-C motif chemokine receptor 4 (CXCR4) is widely expressed in various cells, including immune cells [27]. In immune cells, CXCR4 is mainly responsible for guiding cell migration, helping immune cells home to specific tissue regions, and participating in the regulation of immune responses [28, 29]. In tumor-associated macrophages (TAM), CXCR4 also plays an important role [30]. It participates in regulating the migration of TAM, promoting the aggregation of TAM at the tumor site, and simultaneously affects the activation process and functional state of TAM, as well as the interaction between TAM and other cells, thereby influencing the balance of the immune microenvironment [31,32]. TAM surface CXCR4 can bind to its ligand CXCL12, activating downstream signaling pathways such as the PI3K-Akt pathway [32]. This activation not only promotes TAM migration but also modulates the secretion of cytokines and chemokines, influencing the overall balance of the immune microenvironment. However, the specific regulatory mechanism of CXCR4 + TAM in the immune microenvironment of LUAD, especially the mechanism mediated by inflammation, has not been fully elucidated and urgently requires in-depth study.

Traditional research methods have many limitations in exploring the tumor immune microenvironment and are difficult to comprehensively analyze the interactions between cells and the dynamic changes over time [33, 34]. The rise of bioinformatics has brought new opportunities to this field. Among them, survival prognosis prediction models can predict patients' survival based on a large amount of data, providing a reference for clinical decision-making [35–38]. More importantly, single-cell spatiotemporal analysis technology goes a step further on this basis. It can accurately analyze the state and function of each cell at the single-cell level, determine the specific location of cells in the spatial dimension, and dynamically track the changes of cells in the temporal dimension. It provides strong support for in-depth research on tumor-related mechanisms from multiple dimensions [39–41].

This study employs single-cell and spatial transcriptomic analyses to comprehensively profile the transcriptional landscape of LUAD and normal tissues. The objectives are to delineate the cellular composition and dynamics of the tumor microenvironment, clarify the malignant transformation trajectory of epithelial cells, and analyze the functions of myeloid and T cells along with cell - cell communication. Furthermore, by integrating spatial transcriptomics with in vitro functional experiments, we seek to uncover the specific role of CXCR4 + tumor-associated macrophages (TAMs) and validate the function of key genes. Ultimately, this research aims to define key mechanisms driving LUAD progression and confirm CXCR4 as a promising therapeutic target, thereby providing a foundation for developing more effective treatments.

## 2 Materials and methods

### 2.1 Single-cell sequencing data processing and analysis

Single-cell RNA sequencing data of lung cancer were derived from the article "Single-cell RNA sequencing reveals distinct tumor microenvironment patterns in lung

adenocarcinoma" published by Philip Bischoff and other researcher [42]. Regarding the BULK RNA-seq data, TCGA-LUAD cohort were deposited in The Cancer Genome Atlas Program (TCGA, https://www.cancer.gov/ccg/research/genome-sequencing/tcga), while GSE135222 cohort was downloaded in Gene Expression Ominibus (GEO, https://www.ncbi.nlm.nih.gov/geo/query/acc.cgi ). The original data samples were screened to meet the following criteria: (1) lung adenocarcinoma and adjacent normal lung tissue; (2) the number of cells in each sample was not less than 3000 and not more than 8000. The Seurat package in R software (version 4.3.2) was used to process the raw data of each sample.

scRNA data were processed and analyzed using the Seurat package (v4.2.2) in R. Low-quality cells were excluded based on gene count (< 200 or > 10,000), total counts (< 1,000), and mitochondrial/ribosomal gene content (> 10%), while genes expressed in fewer than three cells were also filtered out. Following "LogNormalize" normalization and identification of 2,000 highly variable genes (HVGs), data were scaled and integrated using the ScaleData function. Principal component analysis (PCA) was performed on the HVGs, and the number of significant principal components was evaluated with the "JackStraw" function. Batch effects were corrected using the Harmony algorithm, and doublets were removed via the scDblFinder package, resulting in the exclusion of 3,714 cells.

### 2.2 Immune infiltration and drug susceptibility analysis

Immune cell composition was performed by CIBERSORT and the TIDE was predicted by Tumor Immune Dysfunction and Exclusion (TIDE, http://tide.dfci.harvard.edu/). Drug susceptibility analysis was performed by "oncoPredict" R package. The TIDE algorithm and drug sensitivity modeling from the GDSC database were employed strictly as exploratory, hypothesis-generating tools to infer potential differences in the tumor immune microenvironment and therapy susceptibility between risk groups.

### 2.3 Pseudotime trajectory analysis

Pseudotime analysis was conducted using the Monocle2 R package. Dimensionality reduction was performed with the "DDRTree" method via the reduceDimension() function, after which cells were ordered along the trajectory using orderCells() to assign pseudotime values. The initial state of the trajectory was automatically determined by the algorithm.

### 2.4 Spatial transcriptomics analysis

The raw spatial transcriptomics sequencing data were quality-controlled and processed using Space Ranger (v1.1) to generate a gene-spot matrix. Subsequent analysis was performed with the Seurat package (v4.2.2). Data were pre-processed by filtering out spots with fewer than 200 detected genes and genes expressed in fewer than 3 spots or with less than 10 total counts. Normalization was conducted using the "LogNormalize" method. Dimensionality reduction was achieved through Principal Component Analysis (PCA), and the top 30 principal components were used for graph-based clustering at a resolution of 1.1. Signature scores, derived from scRNA-seq or spatial transcriptomics data, were calculated using the "AddModuleScore" function with default parameters.

Finally, spatial feature maps were visualized with the "SpatialFeaturePlot" function from Seurat (v4.2.2).

### 2.5 Cell lines and culture

The human lung cell lines A549 (official name: A549; RRID: CVCL_0023; species: Homo sapiens; sex: male; tissue of origin: lung), Calu-3 (official name: Calu-3; RRID: CVCL_0609; species: Homo sapiens; sex: male; tissue of origin: lung), together with the normal cell line BEAS-2B (species: Homo sapiens; tissue of origin: human bronchial epithelial), were obtained from the Shanghai Institute of Cell Biology, Chinese Academy of Science (Shanghai, China) in March 2024.

All cell lines were authenticated by short tandem repeat (STR) profiling, showing a > 90% match to reference profiles obtained from the respective cell banks. Cells were confirmed to be free of mycoplasma contamination prior to experimental use. None of the cell lines used are known to be misidentified or contaminated according to the Cellosaurus database. Cells within 20 passages after thawing were used for all assays. LUAD cell lines were routinely maintained in RPMI-1640 and DMEM (Gibco, USA) medium containing 10% fetal bovine serum (Gibco, USA), 1% streptomycin, and penicillin. All cells were cultured at 37 °C under a 5% $CO_2$ atmosphere in a cell incubator.

### 2.6 Real-time quantitative PCR (RT-qPCR)

Total RNA was obtained employing the TRIzol reagent (Invitrogen). Reverse transcription was performed using the Prime Script TMRT kit (Takara, RR047A) and the Taq II Kit, and PCR amplification was conducted using SYBR Premix Ex according to the manufacturer's instructions. CXCR4 primers utilized were as follows: forward, ACTAC ACCGAGGAAATGGGCT; reverse, CCCACAATGCCAGTTAAGAAGA.

### 2.7 Cell proliferation assay

$5 \times 10^3$ cells were seeded into a single well of a 96-well plate containing 100 μL of complete culture medium. After 24 h, the culture medium was replaced with a full culture medium containing CCK8 reagent. The absorbance was measured at 450 nm after 1, 2, 3, and 4 days.

### 2.8 Colony formation assay

LUAD cells were seeded at a low density of 600 ~ 1000 cells per well in 6-well plates and cultured for approximately 2 weeks. Following the incubation period, the cell colonies were washed with PBS, fixed in 4% paraformaldehyde for 20 min, stained with crystal violet, and documented and enumerated.

### 2.9 EdU (5-Ethynyl-2-deoxyuridine) assay

$2 \times 10^4$ cells were seeded into a single well of a 96-well plate containing 100 μL of complete culture medium. After 24 h, the cells were incubated with EdU reagent according to the manufacturer's instructions, and cell proliferation was measured using a fluorescence microscope (Thermo Fisher Scientific, America).

### 2.10 Invasion assay

The invasion assay was conducted by first trypsinizing the cells, which were then resuspended in a serum-free medium and quantified. A cell suspension was carefully added to the upper chamber of a Transwell insert pre-coated with Matrigel. Following an incubation period of 36 h to allow cell invasion through the Matrigel, the non-invading cells on the upper surface of the insert were gently removed. The invaded cells on the lower surface were fixed with 4% paraformaldehyde, stained with 0.1% crystal violet, and subsequently rinsed with PBS.

### 2.11 Flow cytometry assay

To assess apoptosis, cells ($1 \times 10^6$) were stained with Annexin V-FITC and propidium iodide (PI) apoptosis detection kit (BD Biosciences) according to the manufacturer's instructions. After staining using BD FACS Melody flow cytometry, the percentage of early and late apoptotic cells was assessed.

### 2.12 Statistical analysis

Data are presented as the mean ± standard deviation (SD) of three independent experiments. The R software (version 4.3.0) was used for bioinformatics analysis of data obtained from GEO databases. The expression of CXCR4 and immune infiltration parameters were analyzed using the chi square test and Fisher's exact test. "Log-rank test" for survival curves. All experiments were repeated at least three times ($n = 3$, biological replicates). Intergroup differences were analyzed using Student's t-test or one-way analysis of variance (ANOVA), and statistical analyses were performed with GraphPad Prism 9 software. Significance levels were denoted as follows: $^{*}p < 0.05$, $^{**}p < 0.01$, $^{***}p < 0.001$, and $^{****}p < 0.0001$.

## 3 Results

### 3.1 Quality control and cell classification of LUAD scRNA-seq data

The workflow for this manuscript was summarized in Fig. 1. The single-cell transcriptome dataset utilized in this study is distinguished by its high-quality data and the inclusion of diverse immune cell populations, rendering it an ideal resource for reanalyzing the tumor microenvironment 43. To guarantee the reliability and accuracy of the data, a series of strict quality control criteria were meticulously implemented, a total of 69,867 high-quality cells were retained for subsequent annotation and analysis.

Subsequently, leveraging a comprehensive set of well-established classical cell-type marker genes, these retained cells were systematically classified into eight distinct subgroups. These subgroups include Epithelials, Endothelials, Fibroblasts, Mast cells, Myeloid cells, T cells, B cells, and Plasma cells (Fig. 2A). The marker genes for each cell type were further visualized and validated using dot-plots and feature-plots (Fig. 2B-C). These visualizations not only illustrate the expression levels of marker genes across different cell types but also highlight the specificity of each marker in defining the respective cell populations.

Notably, although all eight cell types were detected in both tumor and normal control samples (Fig. 2A), the proportions of these cell types exhibited substantial differences between the two groups. In the tumor samples, certain cell types showed significant expansion or contraction compared to the normal controls, suggesting a profound

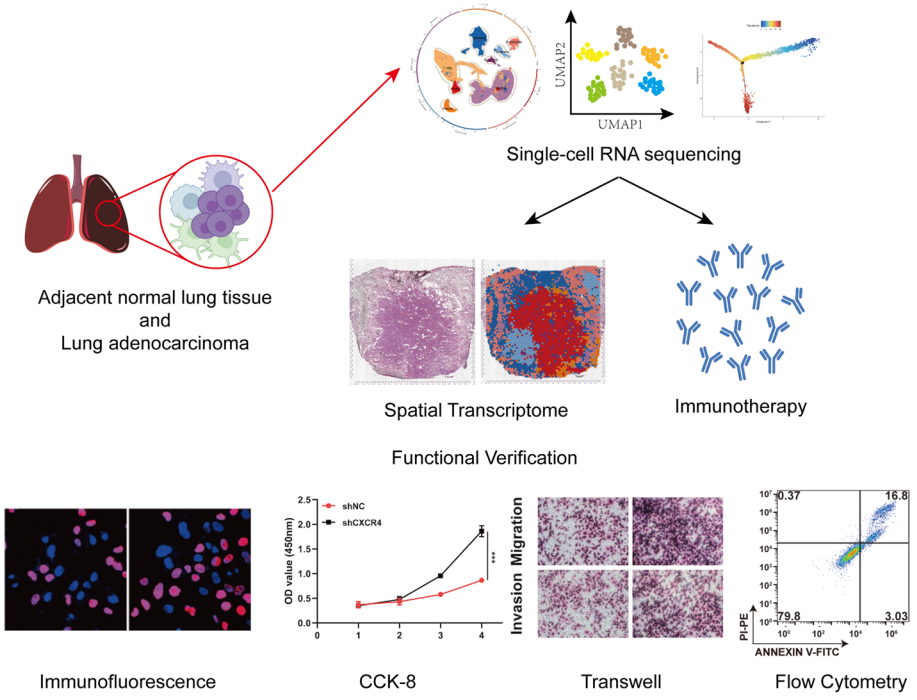


**Fig. 1** Flow chart of the manuscript

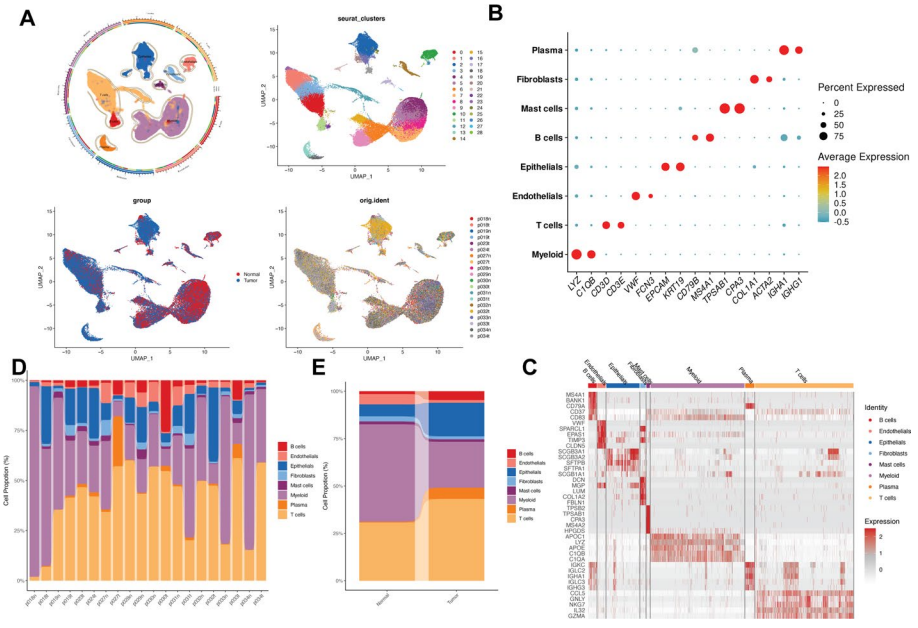


**Fig. 2** Quality Control and Cell Classification of LUAD scRNA-seq Data. **A** UMAP visualization depicting the identification of cell types via scRNA-seq. **B** Expression of canonical cell type markers. **C** Heatmap of feature genes defining cell identities. **D** Inter-sample heterogeneity in cellular composition. **E** Tissue-specific shifts in cell type abundances

remodeling of the cellular composition. This significant alteration in cell-type proportions strongly indicates a modified tumor microenvironment in lung adenocarcinoma, which likely plays a critical role in tumor progression, immune evasion, and response to therapy (Fig. 2D-E). These findings set the stage for further in-depth analyses to explore the functional implications of these changes and their potential as therapeutic targets.

### 3.2 Characterization and trajectory analysis of epithelial cell subpopulations in LUAD

To comprehensively elucidate the progression mechanism of LUAD, we focused our investigation on epithelial cells, as they play a crucial role in the tumor microenvironment. By conducting a subset analysis of these cells, our objective was to uncover the underlying cellular processes that drive the development of LUAD.

Through unsupervised clustering analysis of epithelial cells, we identified 27 distinct cell clusters (Fig. 3A). Our findings revealed that clusters 5, 8, and 13 were predominantly enriched in normal tissues, suggesting their involvement in maintaining the physiological functions of healthy lung tissues. In stark contrast, clusters 0, 1, 2, 3, 4, 7, 9, 10, 14, 15, 16, 17, 18, 19, 20, and 22 were significantly more abundant in tumor samples (Fig. 3A). This differential distribution indicates that these clusters may be closely associated with the malignant transformation and progression of LUAD.

To precisely assess the malignancy of each cell cluster, we employed inferCNV analysis, which is a powerful tool for detecting copy number variations in single cells. By integrating the inferCNV results with sample source information (normal vs. tumor), we were able to accurately classify the cell clusters. Based on the characteristic marker genes of each cluster (Fig. 3B), we identified several subtypes of malignant tumor cells, including $CXCL14^+$ malignant cells, $CXCR4^+$ malignant cells, $HSPA1A^+$ malignant cells, $PLAT^+$ malignant cells, $SCGB3A1^+$ malignant cells, $SPP1^+$ malignant cells, and $TM4SF4^+$ malignant cells (Fig. 3C). The specific marker genes for each cell subtype were visualized in the feature plot, providing a clear depiction of the molecular signatures of these cells (Fig. 3D).

To further explore the developmental trajectories of epithelial cells during LUAD progression, we performed pseudotime trajectory analysis. This analysis allowed us to reconstruct the dynamic changes in cell states and map the potential paths of cell differentiation. Our results clearly delineated two distinct trajectories, with normal and tumor tissues following separate routes (Fig. 3E). According to the pseudotime analysis, all trajectories originated from normal epithelial cells, which then underwent a series of molecular and cellular changes, ultimately leading to the formation of $SPP1^+$ malignant cells (Fig. 3F). This finding suggests that $SPP1^+$ malignant cells may represent the end stage of the malignant transformation process of epithelial cells in LUAD. Functional enrichment analysis indicated that oxidative phosphorylation and ATP synthesis were active in initial stage, while cytoplasmic translation and antigen processing were more active in branch 2 (Fig. 3G).

In conclusion, our study provides a comprehensive understanding of the malignant transformation trajectory of epithelial cells in the LUAD microenvironment. The identification of distinct cell clusters and their associated marker genes, as well as the mapping of developmental trajectories, offers valuable insights into the molecular mechanisms underlying LUAD progression.

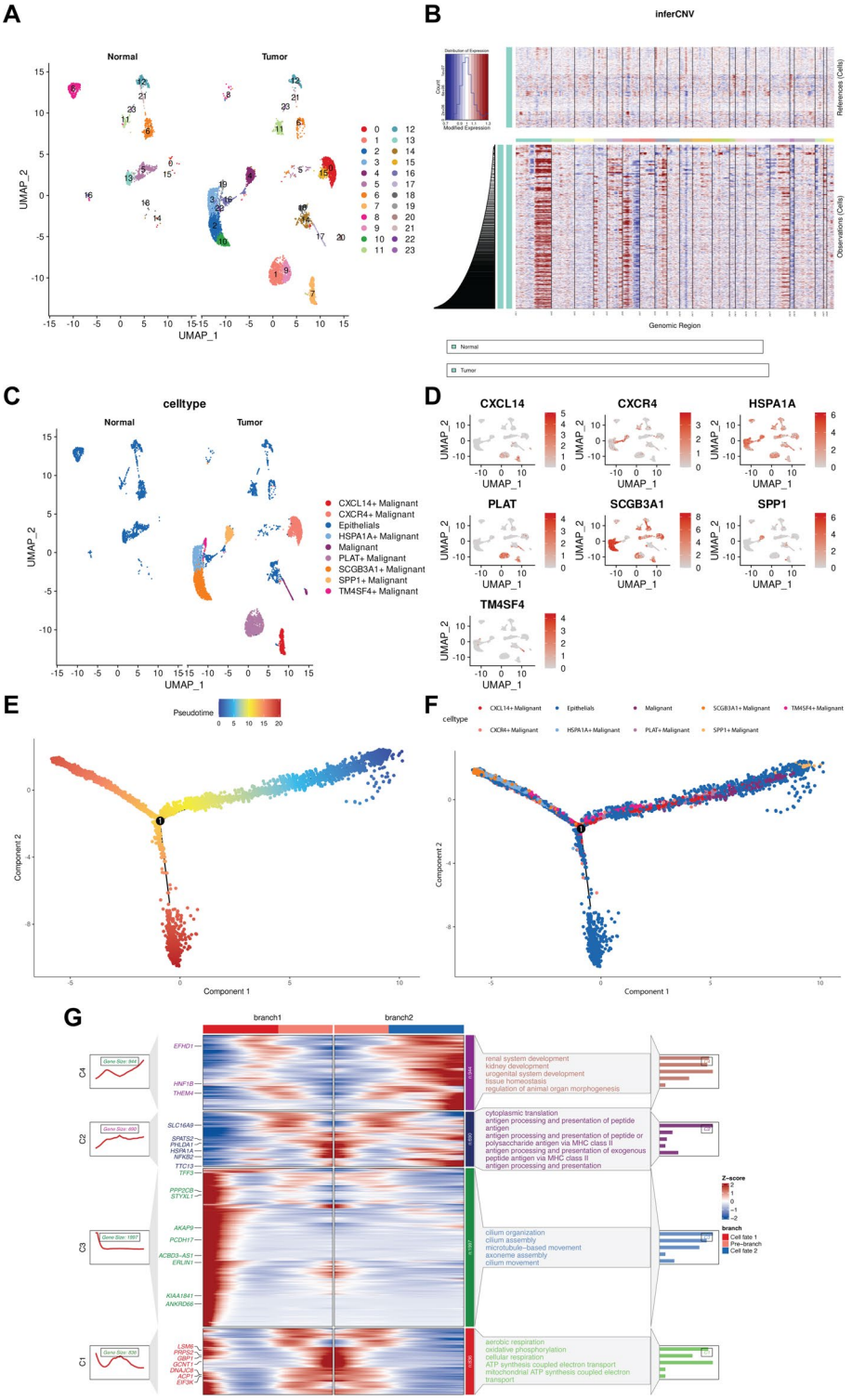


**Fig. 3** Characterization and Trajectory Analysis of Epithelial Cell Subpopulations in LUAD. **A** Malignant cell identification by InferCNV. **B** UMAP visualization of 24 epithelial subclusters. **C** Subcluster distribution across normal and tumor tissues. **D** Spatial expression of feature genes. **E** Pseudotime trajectory of epithelial differentiation. **F** Trajectory variations among tumor subtypes. **G** Gene expression patterns and functional enrichment along trajectories

### 3.3 CXCR4$^+$ TAM is closely associated with poor prognosis in LUAD

Given that myeloid cells constitute a substantial proportion of both tumor and normal samples in our dataset, we conducted an in-depth investigation into their functional characteristics. First, we isolated myeloid cells from the dataset and performed a refined clustering analysis, which resulted in the identification of ten distinct subgroups: CCL18$^+$ macrophage, CCL9$^+$ macrophage, conventional dendritic cell 1 (cDC1), conventional dendritic cell 2 (cDC2), CXCR4$^+$ TAM, FABP4$^+$ macrophage, IL1B$^+$ TAM, macrophage, monocyte, and plasmacytoid dendritic cell (pDC) (Fig. 4A-B). The marker genes highly expressed in each myeloid subpopulation were visualized using dot plots

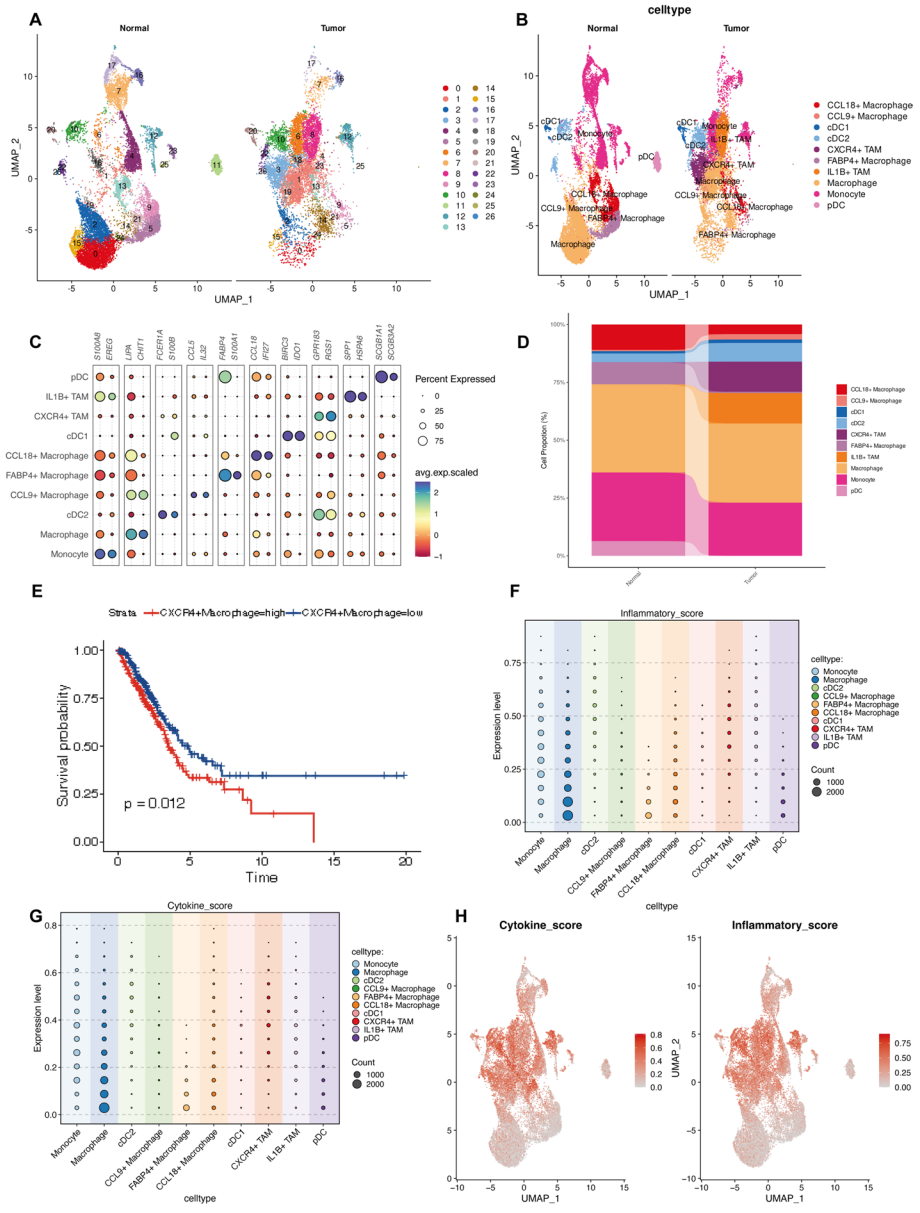


**Fig. 4** CXCR4 +TAM is closely associated with poor prognosis in LUAD. **A** UMAP visualization of 27 myeloid cell subclusters. **B** Distribution of myeloid subpopulations across tissues. **C** Expression of canonical markers for myeloid cell identification. **D** Altered abundance of myeloid subsets in tumor microenvironment. **E** GO enrichment of tumor-associated myeloid cells. **F**–**G** Cytotoxicity **F** and inflammation **G** scores across subsets. **H** UMAP overlay of cytotoxicity scores and inflammatory scores for myeloid cell subpopulations

(Fig. 4C), providing a molecular signature for each cell type. As depicted in the cell proportion plot (Fig. 4D), the relative abundances of CCL18 + macrophage, FABP4$^+$ macrophage, monocyte, macrophage, and pDC were significantly lower in tumor samples compared to normal tissues. Conversely, CCL9$^+$ macrophage, cDC1, cDC2, CXCR4$^+$ TAM, and IL1B$^+$ TAM showed increased proportions in tumor samples, suggesting their potential involvement in tumor-promoting processes.

To elucidate the developmental dynamics of myeloid cells, we performed a pseudotime trajectory analysis. This analysis revealed five distinct developmental trajectories, all of which originated from macrophages and converged towards CXCR4$^+$ TAM (Fig. S1A-B). This finding suggests a hierarchical differentiation pathway within the myeloid cell lineage, potentially indicating the role of CXCR4$^+$ TAM as a terminal effector in the tumor microenvironment.

We then conducted CIBERSORTx for immune deconvolution, using bulk microarray data from TCGA-LUAD. The results showed that elevated infiltration of CXCR4$^+$ macrophages was significantly associated with poorer OS (Fig. 4E). To further explore the functional states of myeloid subpopulations, we calculated the cytokine and inflammatory scores for each cell type. Notably, cDC2, CXCR4$^+$ TAM, and IL1B$^+$ TAM exhibited the highest scores in both cytokine and inflammatory responses (Fig. 4F-G), a conclusion further supported by UMAP visualization (Fig. 4H). These results indicate that these myeloid subpopulations may play a central role in promoting chronic inflammation and tumor progression.

In summary, we identified distinct myeloid cell clusters with differential abundance between tumor and normal tissues, delineated the developmental trajectories leading to CXCR4$^+$ TAM, and revealed the functional significance of specific myeloid subpopulations in regulating the inflammatory tumor microenvironment.

### 3.4 LUAD exhibit a significantly increased infiltration of exhausted CD8 + T cells

Building upon our comprehensive characterization of myeloid cells in the LUAD microenvironment, we next turned our attention to T cells, which also constitute a major component of the tumor immune landscape. Leveraging the same dataset, we isolated T cells and performed a high-resolution re-clustering analysis. This approach led to the identification of twelve distinct T - cell subpopulations: cytotoxic cells, dysfunctional CD8T, effector CD4T, effector CD8T, exhausted CD8T, mucosal-associated invariant T (MAIT) cells, memory CD4T, memory CD8T, naïve T cells, proliferating CD8T, and regulatory T (Treg) cells (Fig. 5A-B). Dot plots were utilized to visualize the marker genes highly expressed in each subpopulation (Fig. 5C), providing a molecular fingerprint for each T cell type.

The cell proportion plot (Fig. 5D) illustrated significant differences in the relative abundances of these T cell subpopulations between tumor and healthy samples. Notably, the proportions of cytotoxic CD8T cells and Treg cells were substantially increased in tumor samples compared to normal tissues, suggesting their active participation in tumor-related immune responses.

To decipher the developmental dynamics of T cells, we employed a pseudotime trajectory analysis. This analysis revealed three distinct developmental trajectories, all of which originated from Naïve T cells and terminated at Dysfunctional CD8T and Treg

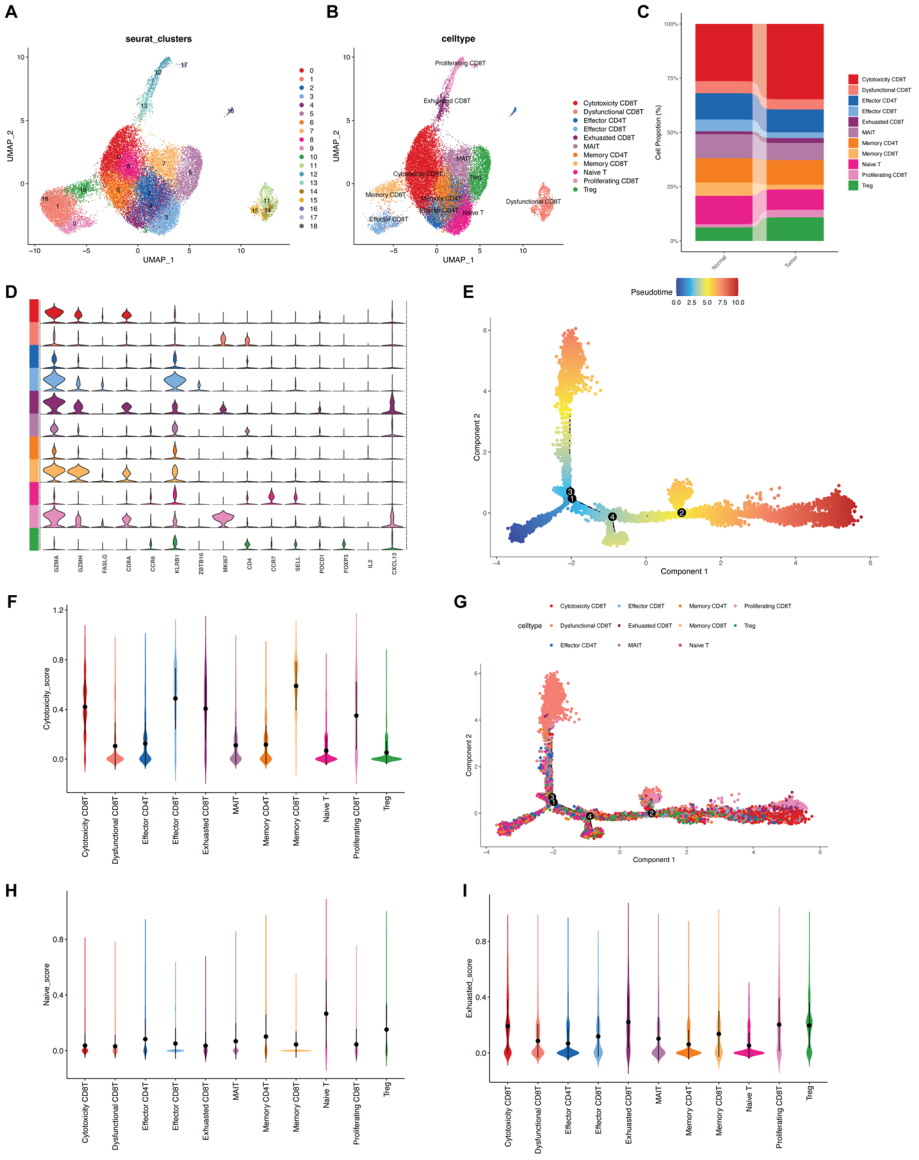


**Fig. 5** LUAD exhibit a significantly increased infiltration of exhausted CD8+T cells. **A** UMAP visualization of 19 T cell subclusters. **B** Tissue distribution of T cell subpopulations. **C** Canonical marker expression for T cell subset identification. **D** Altered abundance of T cell subsets in tumor microenvironment. **E** Pseudotime trajectory of T cell differentiation. **F** Lineage variations among tumor T cell subtypes. **G**–**I** Cytotoxicity **G**, naïve **H**, and exhaustion (**I**) scores across T cell subsets

(Fig. 5E-F). This finding implies a potential developmental hierarchy within the T cell compartment.

To further validate our observations, we are currently in the process of calculating cytokine, naïve, and exhausted scores for each T cell subpopulation (Fig. 5G-I). These scores will provide additional insights into the functional states of T cells and help elucidate their roles in shaping the tumor immune microenvironment. Our ongoing analyses aim to comprehensively understand the complex interplay between different T cell subpopulations and their contributions to LUAD progression, which may guide the development of more effective immunotherapeutic strategies.

### 3.5 Intercellular communication networks unveil pathogenesis and therapeutic targets in LUAD

Building on our detailed characterization of individual cell types and their developmental trajectories in LUAD, we next sought to explore the complex landscape of cell-cell communication within the tumor microenvironment. To achieve this, we employed CellChatDB, a meticulously curated database that compiles literature-supported ligand-receptor interactions.

The overall cell-cell communication network was first visualized using a circular plot, which depicted the number of interactions and their corresponding weights/strengths among different cell populations (Fig. 6A). Given the complexity of the communication network, we further dissected the signaling patterns originating from each cell group. This analysis revealed a particularly robust interaction network between epithelial cells and myeloid cells (Fig. 6B), suggesting a significant crosstalk between these two cell types that likely influences tumor progression. To highlight key molecular interactions, we generated a bubble plot, which emphasized the importance of specific signaling pathways such as SCGB3A2-MARCO and APP-CD74 in mediating communication between epithelial and myeloid cells (Fig. 6C).

Guided by our previous pseudotime analysis, which implicated CXCR4 in tumorigenesis and development, we focused on identifying the cell types engaged in active CXCR-CXCL signaling. Consistent with our earlier findings, the CCL signaling pathway was found to be highly active among fibroblast cells, T cells, and myeloid cells (Fig. 6D), underscoring the role of these signaling axes in coordinating cellular functions within the tumor microenvironment.

To provide a holistic view of the interrelationships among all cell populations, we constructed a correlation heatmap. This analysis not only validated our previous observations but also revealed that $CXCR4^+$ TAM exhibited significant correlations with tumor cells and other immune cell types (Fig. 6E). Collectively, our analysis of intercellular communication networks provides critical insights into the molecular mechanisms underlying LUAD pathogenesis and may inform the development of novel therapeutic strategies targeting cell-cell interactions.

### 3.6 Spatial organization of cell subpopulations reveals functional interplay in LUAD Tissues

Building on our understanding of cellular composition, developmental trajectories, and intercellular communication in LUAD, we further explored the spatial organization of cell type subpopulations within tumor tissues. The dataset (GSE189487) of Lung Adenocarcinoma, retrieved from the Gene Expression Omnibus (GEO) database, encompasses samples derived from patients diagnosed with lung adenocarcinoma and normal individuals [43]. Leveraging spatial transcriptomics, we analyzed tissue sections from both cancerous and normal vasculature regions of LUAD patients. Based on the unbiased clustering and spot features for resolution as 1, we classified the spatial transcriptomic spots into seven distinct cell clusters: malignant cells, epithelial cells, myeloid cells, fibroblasts, $CXCR4^+$ TAM, $SPP1^+$ malignant cells, as well as T and B cells (Fig. 7A). In the co-localization region of malignant cells and macrophages, we screened out capture points where the SPP1/CXCR4 expression level was 25% higher than a specific threshold, which were defined as CXCR4 + TAM/SPP1 + Malignant Spot. The spatial distribution patterns

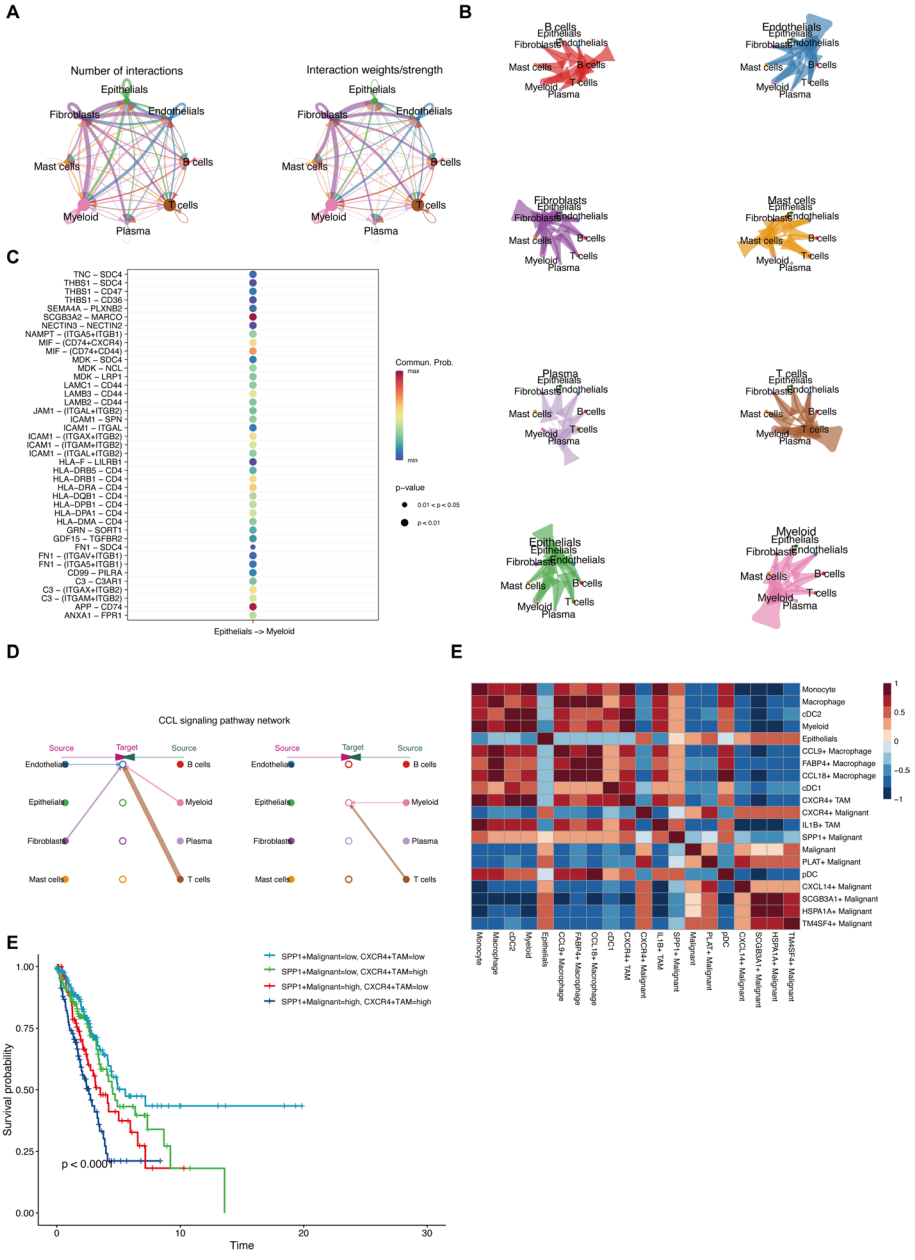


**Fig. 6** Intercellular Communication Networks Unveil Pathogenesis and Therapeutic Targets in LUAD. **A** Interactions weights and strengths between cell types. **B** Specific cell-type communication patterns. **C** Signaling between epithelial and myeloid cells. **D** The communication network of the CCL signaling pathway. **E** Correlation analysis of cellular subpopulations. **F** OS survival analysis on four group of TCGA-LUAD

of these seven cell types were visualized in Fig. 7B7 providing a comprehensive overview of their localization within the tissue microenvironment.

To validate the accuracy of the spatial classification, we examined the expression of specific marker genes for each cell type (Fig. 7C). Notably, we identified spatial spots that co-expressed CXCR4, SPP1, and EPCAM, indicating the spatial co-localization of these key molecules (Fig. 7D-F), with higher expression levels highlighted in red. Furthermore, the signature scores of $CXCR4^{+}$ TAM and $SPP1^{+}$ malignant cells exhibited a significant positive correlation (Fig. 7G), suggesting a potential functional interplay between these cell populations in the tumor microenvironment. Additionally, we also visualized the

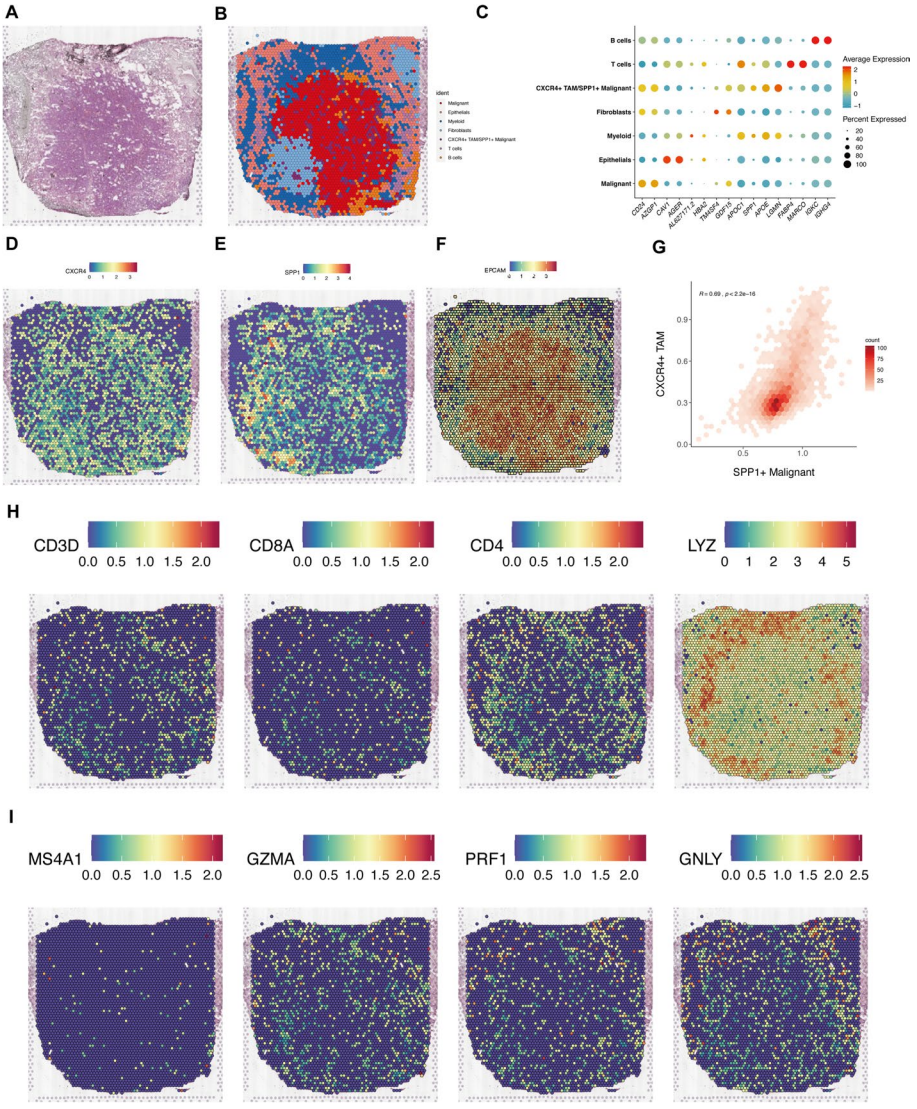


**Fig. 7** Spatial Organization of Cell Subpopulations Reveals Functional Interplay in LUAD Tissues. **A** H&E staining of spatial transcriptomics (ST) section. **B** Unbiased clustering of cell types across ST spots. **C** Cluster identity defined by canonical markers. **D**–**F** Spatial localization of CXCR4 (**D**), SPP1 **E**, and EPCAM **F** expression. **G** Correlation between SPP1$^{+}$ malignant and CXCR4$^{+}$ TAM spatial signatures. **H** Spatial feature representing the gene expression levels of CD3D, CD8A, CD4 and LYZ. **I** Spatial feature representing the gene expression levels of MS4A1, GZMA, PRF1 and GNLY

expression of classic T cell markers (Fig. 7H-I), contributing to a more complete understanding of the spatial immune cell landscape in LUAD.

### 3.7 The heterogeneity of immunotherapy and immune infiltration between SPP1$^{+}$ Malignant$^{high}$/CXCR4$^{+}$TAM$^{high}$ and SPP1$^{+}$ Malignant$^{low}$/CXCR4$^{+}$TAM$^{low}$

To further investigate the heterogeneity of SPP1$^{+}$ Malignant$^{high}$/CXCR4$^{+}$TAM$^{high}$ and SPP1$^{+}$ Malignant$^{low}$/CXCR4$^{+}$TAM$^{low}$, 22 immune cell components were calculated for each patient using the "ssGSEA" methods. Among these immune cells, CD8T cells and Macrophage M0 were highly expressed in the SPP1$^{+}$ Malignant$^{low}$/CXCR4$^{+}$TAM$^{low}$ group (Fig. 8A-B), while the low infiltration group were low expression. These results suggest that the reason for better prognosis in the low infiltration group may be related

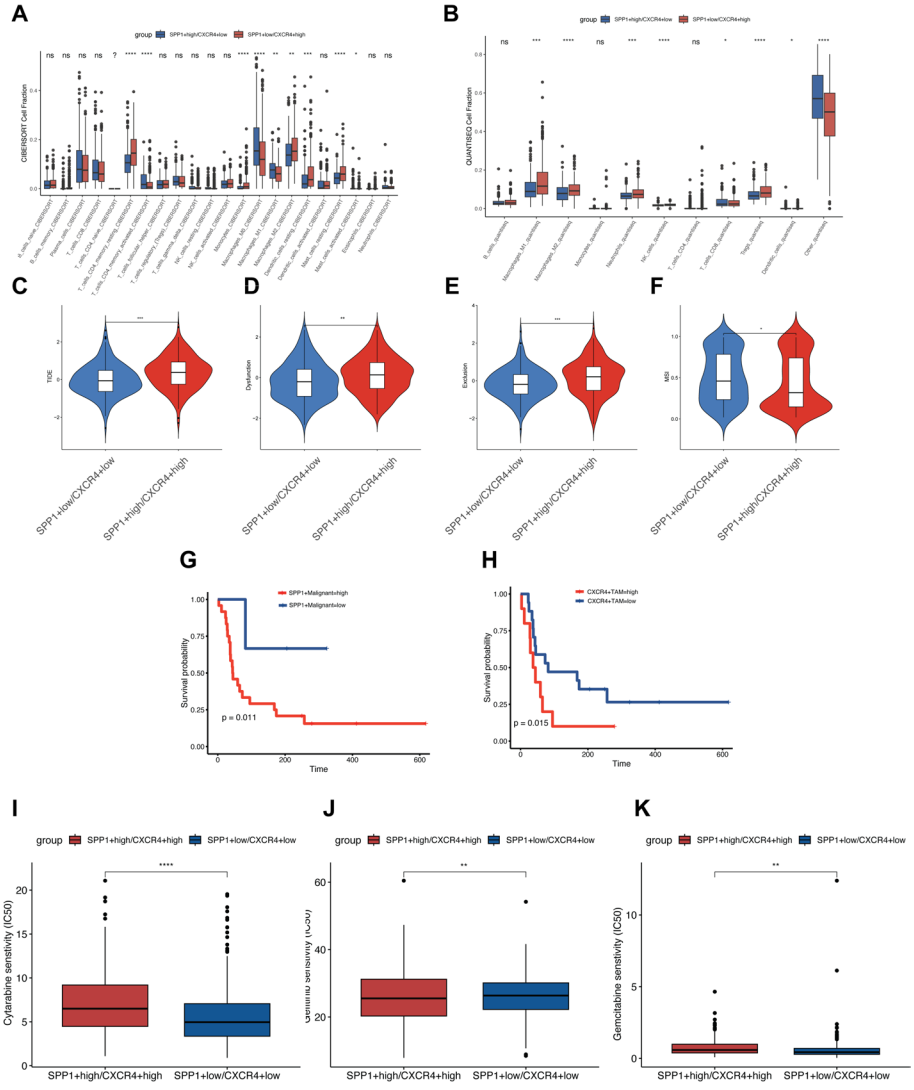


**Fig. 8** The heterogeneity of immunotherapy and immune infiltration between SPP1$^+$ Malignant$^{high}$/CXCR4$^+$TAM$^{high}$ and SPP1$^+$ Malignant$^{low}$/CXCR4$^+$TAM$^{low}$. **A** The proportion of immune cells in SPP1$^+$ malignant /CXCR4$^+$ TAM low and high infiltration samples in CIBERSORT algorithm. **B** The proportion of immune cells in SPP1$^+$ malignant / CXCR4$^+$ TAM low and high infiltration samples in QUANTISEQ algorithm. (C-F) The TIDE score **C** Dysfunctional score **D** Exclusion score **E** and MSI score **F** in two groups. **G**–**H** KM plot of SPP1 + infiltration of GSE135222 **G** KM plot of CXCR4 + infiltration of GSE135222. **I**–**K** The heterogeneity of Cytarabine **I** Gefitinib **J** Gemcitabine **K** drug sensitivity in two groups

to the immune microenvironment and have a higher level of immune infiltration in LUAD. At the same time, we evaluated the effect of low and high infiltration on TIDE score, Dysfunction score, Exclusion score, and MSI score using the "TIDE" algorithm. The result showed that the TIDE score, Dysfunction score, Exclusion score in SPP1$^+$ Malignant$^{high}$/CXCR4$^+$TAM$^{high}$ were significantly increased, while the MSI score was relatively low. (Fig. 8C-F). This indicated that the immune escape potential of patients in high infiltration increased, and the efficacy of immune checkpoint suppressive therapy might be poorer. To validate the results, we performed the high and low infiltration with the GSE135222 dataset. SPP1$^+$ Malignant$^{high}$ and CXCR4$^+$TAM$^{high}$ patients showed shorter survival time than SPP1$^+$ Malignant$^{low}$ and CXCR4$^+$TAM$^{low}$, individually (Fig. 8G-H). Finally, Drug susceptibility prediction via "oncoPredict" R package indicated

that IC50 values for Cytarabine and Gemcitabine were significantly lower in high infiltration group, while Gefitinib had the opposite trend (Fig. 8I-K).

### 3.8 Validation of CXCR4-driven LUAD progression in vitro

To translate our in-silico and spatial findings into functional insights, we conducted a series of in vitro experiments to validate the role of key genes in LUAD progression. Given the critical role of CXCR4 identified in our previous analyses, we first examined its expression levels in three lung cell lines. Quantitative analysis revealed that the A549 cell line exhibited an approximately 8-fold increase in CXCR4 expression compared to a reference control (BEAS-2B cell lines) (Fig. 9A).

Subsequently, we employed knockdown the CXCR4 mRNA to investigate the impact of CXCR4 on tumor cell behavior (Fig. 9B). The results of the CCK-8 assay indicated that knockdown of CXCR4 significantly enhanced cell viability (Fig. 9C), suggesting that lung cancer cells with low expression of CXCR4 might enhance their survival ability by evading the killing effect of $CXCR4^{+}$ TAM. Consistent with this finding, colony formation assays demonstrated that CXCR4-knockdown cells formed a greater number of colonies with larger sizes (Fig. 9D), indicating enhanced proliferative capacity. The EdU assay demonstrated that compared with the shNC group, the EdU positive cell rates of A549 and Calu-3 cell lines treated with shCXCR4 were significantly increased, which also indicated that knockdown of CXCR4 could promote the cell proliferation of these two cell lines (Fig. 9E).

To assess the role of CXCR4 in tumor cell invasion and migration, we performed Transwell assays. The results showed that the knockdown of CXCR4 significantly enhanced the invasive and migratory abilities of A549 and Calu-3 cells (Fig. 9F), highlighting its importance in the metastatic potential of LUAD cells. Finally, flow cytometry analysis revealed that CXCR4 knockdown inhibited apoptosis in lung cancer cells (Fig. 9G), further emphasizing the multifaceted role of CXCR4 in regulating tumor cell fate. Through GSEA analysis of the samples of CXCR4 + TAM-high and CXCR4 + TAM-low, the results showed that the glycolytic pathway was significantly upregulated and the immune response was significantly downregulated in the CXCR4 + TAM-high group (Fig. 9H). These in vitro findings provide strong functional evidence supporting the significance of CXCR4 in LUAD development and progression, laying the foundation for future therapeutic interventions targeting this molecule. Tumor cell intrinsic CXCR4 may act as a "metabolic checkpoint" that restrains glycolysis. Its knockdown releases this brake, triggering Warburg-effect reprogramming. This metabolic shift creates a lactate-rich, glucose-depleted microenvironment that drives the polarization and immunosuppressive function of CXCR4 + TAMs, ultimately leading to both enhanced tumor proliferation and CD8 + T cell suppression.

## 4 Discussion

According to the 2020 GLOBOCAN statistics, there were approximately 2.2 million new cases of lung cancer each year, ranking second in incidence and first in mortality, accounting for 18% of all cancer deaths, with an extremely high degree of malignancy [44]. Despite the continuous advancement of screening and treatment methods, due to the large number of patients and high heterogeneity, most patients are diagnosed at the middle or advanced stage, resulting in a five-year survival rate of less than 20% for

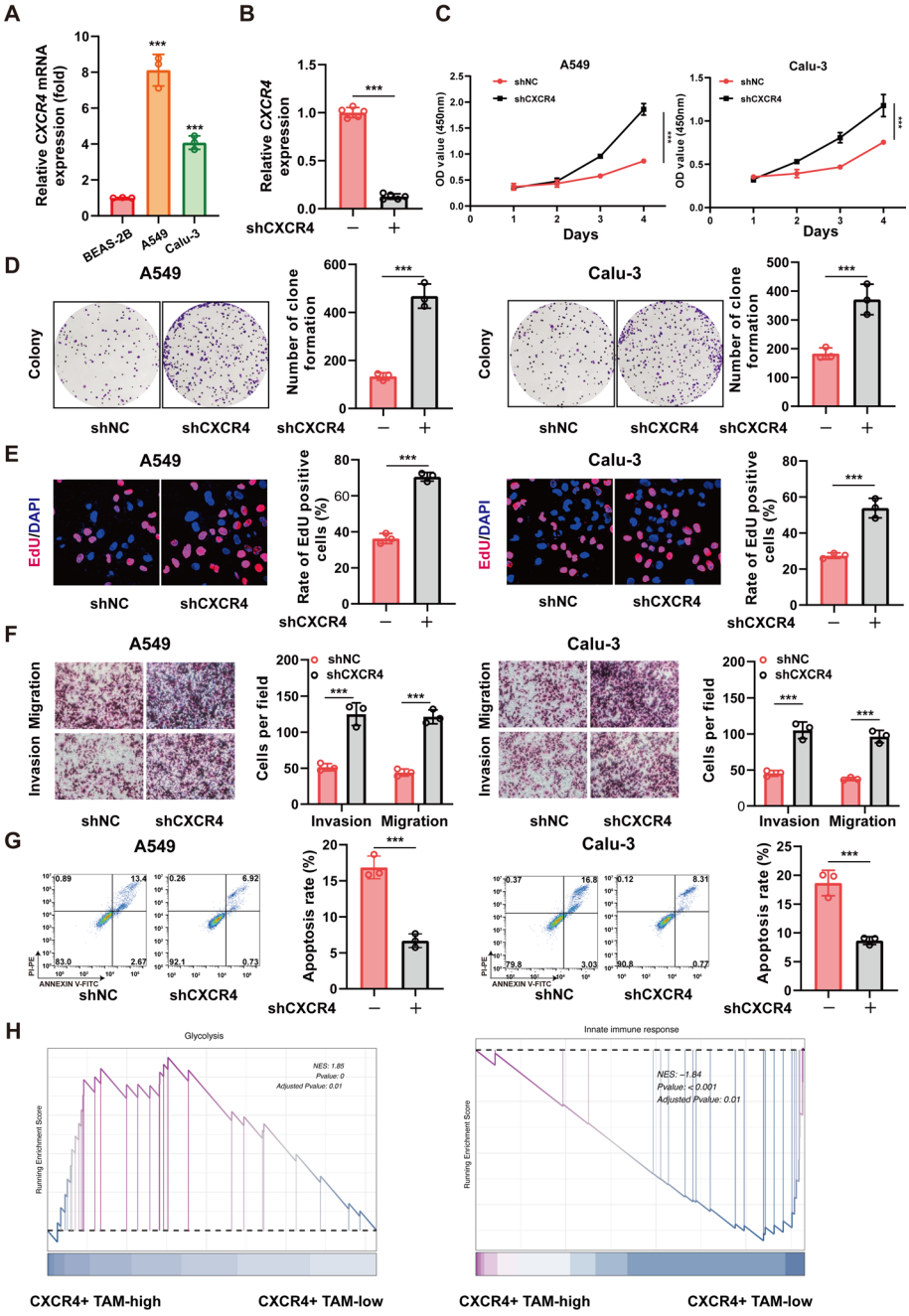


**Fig. 9** Validation of CXCR4-Driven LUAD Progression In Vitro. **A** RT-PCR analysis of CXCR4 mRNA expression levels in four human LUAD cell lines ($n = 3$, $p < 0.05$, t-test). **B** Knockdown efficiency validation of CXCR4 by RT-PCR ($n = 5$, $p < 0.05$, t-test). **C** CCK-8 assay to evaluate the effects of CXCR4 knockdown on cell viability in LUAD cells ($n = 3$, $p < 0.05$, t-test). **D** Colony formation assay to assess the impact of CXCR4 knockdown on cell proliferation, with quantification of results ($n = 3$, $p < 0.05$, t-test). **E** EdU assay for detecting DNA synthesis activity in LUAD cells with CXCR4 knockdown ($n = 3$, $p < 0.05$, t-test). **F** Transwell invasion assay demonstrating the effects of CXCR4 knockdown on cell invasion, with quantification of results ($n = 3$, $p < 0.05$, t-test). **G** Flow cytometry analysis of apoptosis rates in LUAD cells with CXCR4 knockdown, including quantification of results ($n = 3$, $p < 0.05$, t-test). **H** Gene sets enrichment analysis of CXCR4 + TAM-high and CXCR4 + TAM-low

non-small cell lung cancer [45]. For LUAD patients who are not suitable for surgery, targeted and immunotherapy offer new options. Although PD-1/PD-L1 inhibitors and others can activate immunity by regulating the tumor microenvironment, their efficacy varies from person to person [46]. Therefore, developing biomarkers for predicting therapeutic efficacy and prognosis is the key to promoting precision medicine and optimizing patient diagnosis and treatment. The CXCR4/CXCL12 axis plays a crucial role in various solid tumors such as lung cancer, liver cancer, and breast cancer, and can promote the migration, invasion, and distant metastasis of cancer cells. Furthermore, studies have shown that CXCR4 inhibitors can significantly improve the tumor microenvironment of pancreatic cancer and enhance the tumor's sensitivity to immune checkpoint inhibitors, thereby improving the efficacy of immunotherapy. For this reason, CXCR4 is regarded as a promising immune-related prognostic marker. However, its value in the evaluation of tumor immune prognosis, especially in lung adenocarcinoma, has not been fully explored. LUAD poses a significant global health challenge with dismal survival rates. Previous research has highlighted the importance of the immune microenvironment, inflammation, and specific cell types like TAM in LUAD progression [47, 48]. However, traditional research methods often lack the ability to comprehensively analyze dynamic cell-cell interactions and temporal changes in the tumor microenvironment. Existing studies on the regulatory mechanism of $CXCR4^+$ TAM, especially in the context of inflammation in LUAD, remain incomplete, hindering the development of targeted therapies.

We successfully characterized the cell composition of LUAD and normal tissues, revealing substantial differences in cell-type proportions. For epithelial cells, we identified specific malignant cell subtypes and demonstrated that $SPP1^+$ malignant cells may be the end - stage product of epithelial cell transformation. In myeloid cells, we found that $CXCR4^+$ TAM is the terminal effector in a hierarchical differentiation pathway and plays a crucial role in promoting inflammation. For T cells, we discovered a potential developmental hierarchy from NK cells to Treg cells. The intercellular communication analysis revealed strong interactions between epithelial and myeloid cells, with $CXCR4^+$ TAM as a key regulator.

Despite these achievements, our study has limitations. The in vitro experiments only used a limited number of cell lines, which may not fully represent the complexity of LUAD in vivo. Additionally, the mechanisms by which $CXCR4^+$ TAM regulates the immune microenvironment through inflammation are not fully explored. Future research could expand the scope of in vitro and in vivo models, investigate the detailed molecular mechanisms of CXCR4 - mediated inflammation, and explore the feasibility of developing CXCR4-targeted drugs in combination with other immunotherapies to improve LUAD treatment outcomes.

Our study innovatively applies single-cell spatiotemporal analysis to decipher the transcriptomic landscape of LUAD. This approach enabled the precise delineation of cellular heterogeneity, trajectory of epithelial cell malignant transformation, and the functional dynamics of myeloid and T cells. By integrating spatial transcriptomics with in vitro validation, we uncover the pivotal role of CXCR4 + tumor-associated macrophages, thereby nominating CXCR4 as a promising therapeutic target and providing a multidimensional perspective beyond previous single-level analyses. Moreover, our study unveils a targetable immune-suppressive point driven by the SPP1/CXCR4 axis, offering a rational

roadmap for novel combination therapies in LUAD. Specifically, our data provide a rationale for combining CXCR4 blockade with current anti-PD-1/PD-L1 immunotherapy. This strategy concurrently targets immune evasion, dismantling the key immunosuppressive niche by preventing TAM recruitment and potentially reprogramming their function. Importantly, the SPP1/CXCR4 + signature identified here could serve as a predictive biomarker to enrich for patients most likely to benefit from such a combination, moving towards a more personalized treatment approach. These findings have significant implications for the development of novel treatment strategies for LUAD. Our findings reveal that the SPP1/CXCR4 axis in LUAD exhibits mechanistic distinctions from its roles in other cancers. Firstly, in contrast to head and neck squamous cell carcinoma where stromal fibroblasts are key SPP1 sources [49], we identify SPP1 + Malignant as the predominant contributor, indicating a cell-type-specific reprogramming inherent to the LUAD TME. This integrated pathway aligns with the oncogenic signaling architecture and immune evasion priorities of LUAD, differing from the metastasis-centric role described in hepatocellular carcinoma [50].

In vitro knockdown of CXCR4 in LUAD cell lines unexpectedly enhanced their proliferative, invasive, and pro-survival capacities. This apparent contradiction likely reflects the profound cell type specific and context dependent duality of CXCR4 signaling. In the TME, CXCR4 expression on TAMs is central to their recruitment and polarization, establishing a dominant immunosuppressive niche that drives progression. Conversely, within cancer cells, CXCR4 may engage in autocrine or feedback loops that, in certain contexts, restrain hyper-proliferative pathways or prime cells for apoptosis; its loss in vitro could thus release this intrinsic brake. This duality underscores that CXCR4 is not a simple 'on' or 'off' switch for cancer but a context-dependent regulator. Future studies employing cell type–specific knockout models are essential to disentangle these compartment-specific functions for therapeutic targeting. This duality can be reconciled by considering established mechanisms: the CXCR4/CXCR7 dual-receptor system, where CXCR7 can scavenge the shared ligand CXCL12 and modulate signaling outcomes [51] and ligand-independent or biased signaling regulated by the cellular context [52]. Consequently, the in vitro phenotype may reveal a cell-intrinsic, context-specific regulatory function of CXCR4 that is dominated in vivo by its overarching role in recruiting immunosuppressive $CXCR4^{+}$ TAMs. This refined perspective, grounded in existing literature, underscores the complexity of CXCR4 biology and highlights the necessity for future studies employing cell type-specific models to dissect its compartmentalized functions in tumor progression. In early-stage lesions, CXCR4 may guide macrophage recruitment to sites of initial immune activity, where signals like IFN-γ could transiently polarize them toward a pro-inflammatory state [53]. However, as the tumor advances, chronic exposure to factors such as hypoxia, TGF-β, and lactate within an established TME reprograms CXCR4 + TAMs into a stably immunosuppressive phenotype that facilitates immune evasion and progression [54]. This stage-specific plasticity is supported by single-cell studies showing shifting chemokine receptor profiles in LUAD macrophages and functional data demonstrating CXCR4 dependent unidirectional transition of monocytes into pro-metastatic macrophages [31]. Therefore, our findings illuminate the dominant role of this axis in advanced disease. Our study is the tumor cell-intrinsic expression and function of SPP1 in LUAD progression, which underscores a critical, context-dependent duality of this multifunctional cytokine. This observation invites a

direct comparison with other malignancies, such as head and neck squamous cell carcinoma (HNSCC) and hepatocellular carcinoma (HCC), where the predominant cellular source and consequent biological impact of SPP1 diverge significantly, highlighting the cell-type specificity of the SPP1 signaling axis. This nuanced understanding underscores that therapeutic targeting of CXCR4 + TAMs must be contextual, prioritizing patients with advanced, immunosuppressive TMEs where this pathway is actively driving immune suppression. A key limitation of our study, our computational predictions of an $SPP1^+$ Malignant and $CXCR4^+$ TAM axis were not validated by direct experimental evidence. While our bioinformatic analyses strongly suggest interaction between $SPP1^+$ Malignant and $CXCR4^+$ TAMs, we did not perform ligand-receptor binding assays, co-culture systems, or antibody-blocking experiments to conclusively demonstrate a physical and functional interaction. Moreover, the precise functional consequences and the downstream signaling cascades that mediate this effect remain an open question, as we did not perform functional assays to directly test T-cell functionality. We are collaborating with Lab LU to perform ligand-receptor binding assays, co-culture systems, or antibody-blocking experiments to conclusively demonstrate a physical and functional interaction by Q3 2026.

**Abbreviations**

| | |
|---|---|
| TAMs | Tumor-associated macrophages |
| GO | Gene ontology |
| KEGG | Kyoto Encyclopedia of Genes and Genomes |
| IC50 | Half-maximal inhibitory concentration |
| TIDE | Tumor immune dysfunction and exclusion |
| LASSO | Least absolute shrinkage and selection operator |
| DEGs | Differentially expressed genes |

## Supplementary Information

The online version contains supplementary material available at https://doi.org/10.1007/s12672-026-05095-w.

Supplementary Material 1.

**Author contributions**

Beili Wang and Juanwen Lian wrote the main manuscript text and prepared all figures and tables. Jialing Xu and Tao Hua performed the experiments. Jie Ding and Tuo Wang analyzed the data. Cong Cao and Zejie Liu contributed to the study design and methodology. All authors reviewed and approved the final manuscript.

**Funding**

The authors received no financial support for the research, authorship, and publication of this article.

**Data availability**

The datasets analyzed during the current study are available in online repositories: https://www.ncbi.nlm.nih.gov/geo/; GSE135222 and the UCSC/ TCGA-Hub repository, https://xenabrowser.net/datapages/; TCGA-LUAD. Code is available at https://github.com/Hard-Song/multi_omics_LUAD.git.

## Declarations

**Ethics approval and consent to participate**

This article does not contain any studies with human or animal participants.

**Consent for publication**

Not applicable.

**Competing interests**

The authors declare no competing interests.

Received: 18 August 2025 / Accepted: 23 April 2026

Published online: 28 April 2026

**References**


1. Thai AA, Solomon BJ, Sequist LV, Gainor JF, Heist RS. Lung cancer. Lancet. 2021;398:535–54. https://doi.org/10.1016/s0140-6736(21)00312-3.
2. Nicholson AG, et al. The 2021 WHO Classification of Lung Tumors: Impact of Advances Since 2015. J Thorac Oncol. 2022;17:362–87. https://doi.org/10.1016/j.jtho.2021.11.003.
3. Succony L, Rassl DM, Barker AP, McCaughan FM, Rintoul RC. Adenocarcinoma spectrum lesions of the lung: Detection, pathology and treatment strategies. Cancer Treat Rev. 2021;99:102237. https://doi.org/10.1016/j.ctrv.2021.102237.
4. Borczuk AC. Updates in grading and invasion assessment in lung adenocarcinoma. Mod Pathol. 2022;35:28–35. https://doi.org/10.1038/s41379-021-00934-3.
5. Cha MK, Kim IH. Preferential overexpression of glutaredoxin3 in human colon and lung carcinoma. Cancer Epidemiol. 2009;33:281–7. https://doi.org/10.1016/j.canep.2009.08.006.
6. Liu X, Cho WC. Precision medicine in immune checkpoint blockade therapy for non-small cell lung cancer. Clin Transl Med. 2017;6:7. https://doi.org/10.1186/s40169-017-0136-7.
7. Yi M, et al. Biomarkers for predicting efficacy of PD-1/PD-L1 inhibitors. Mol Cancer. 2018;17:129. https://doi.org/10.1186/s12943-018-0864-3.
8. Qian J et al. A CXCR4 partial agonist improves immunotherapy by targeting immunosuppressive neutrophils and cancer-driven granulopoiesis. *Cancer Cell* 43, 1512–1529.e1511 (2025). https://doi.org/10.1016/j.ccell.2025.06.006
9. Kim N, et al. Single-cell RNA sequencing demonstrates the molecular and cellular reprogramming of metastatic lung adenocarcinoma. Nat Commun. 2020;11:2285. https://doi.org/10.1038/s41467-020-16164-1.
10. He A, et al. TYK2 is a prognostic biomarker and associated with immune infiltration in the lung adenocarcinoma microenvironment. Asia Pac J Clin Oncol. 2022;18:e129–40. https://doi.org/10.1111/ajco.13569.
11. Zavitsanou AM, et al. KEAP1 mutation in lung adenocarcinoma promotes immune evasion and immunotherapy resistance. Cell Rep. 2023;42:113295. https://doi.org/10.1016/j.celrep.2023.113295.
12. Lv B, et al. Immunotherapy: Reshape the Tumor Immune Microenvironment. Front Immunol. 2022;13:844142. https://doi.org/10.3389/fimmu.2022.844142.
13. Gajewski TF, Schreiber H, Fu YX. Innate and adaptive immune cells in the tumor microenvironment. Nat Immunol. 2013;14:1014–22. https://doi.org/10.1038/ni.2703.
14. Lei X, et al. Immune cells within the tumor microenvironment: Biological functions and roles in cancer immunotherapy. Cancer Lett. 2020;470:126–33. https://doi.org/10.1016/j.canlet.2019.11.009.
15. Greten FR, Grivennikov SI. Inflammation and Cancer: Triggers, Mechanisms, and Consequences. Immunity. 2019;51:27–41. https://doi.org/10.1016/j.immuni.2019.06.025.
16. Khan M, et al. Pyroptosis relates to tumor microenvironment remodeling and prognosis: A pan-cancer perspective. Front Immunol. 2022;13:1062225. https://doi.org/10.3389/fimmu.2022.1062225.
17. Singh N, et al. Inflammation and cancer. Ann Afr Med. 2019;18:121–6. https://doi.org/10.4103/aam.aam_56_18.
18. Diakos CI, Charles KA, McMillan DC, Clarke SJ. Cancer-related inflammation and treatment effectiveness. Lancet Oncol. 2014;15:e493–503. https://doi.org/10.1016/s1470-2045(14)70263-3.
19. Martinez-Terroba E, et al. Overexpression of Malat1 drives metastasis through inflammatory reprogramming of the tumor microenvironment. Sci Immunol. 2024;9:eadh5462. https://doi.org/10.1126/sciimmunol.adh5462.
20. Owen KL, Brockwell NK, Parker BS. JAK-STAT Signaling: A Double-Edged Sword of Immune Regulation and Cancer Progression. Cancers (Basel). 2019;11. https://doi.org/10.3390/cancers11122002.
21. de Carvalho TG, et al. Inhibition of murine colorectal cancer metastasis by targeting M2-TAM through STAT3/NF-kB/AKT signaling using macrophage 1-derived extracellular vesicles loaded with oxaliplatin, retinoic acid, and Libidibia ferrea. Biomed Pharmacother. 2023;168:115663. https://doi.org/10.1016/j.biopha.2023.115663.
22. DiDonato JA, Mercurio F, Karin M. NF-κB and the link between inflammation and cancer. Immunol Rev. 2012;246:379–400. https://doi.org/10.1111/j.1600-065X.2012.01099.x.
23. Ruf B, et al. Tumor-associated macrophages trigger MAIT cell dysfunction at the HCC invasive margin. Cell. 2023;186:3686–e37053632. https://doi.org/10.1016/j.cell.2023.07.026.
24. Liu Y, Li L, Li Y, Zhao X. Research Progress on Tumor-Associated Macrophages and Inflammation in Cervical Cancer. Biomed Res Int. 2020;2020(6842963). https://doi.org/10.1155/2020/6842963.
25. Lavy M, Gauttier V, Poirier N, Barillé-Nion S, Blanquart C. Specialized Pro-Resolving Mediators Mitigate Cancer-Related Inflammation: Role of Tumor-Associated Macrophages and Therapeutic Opportunities. Front Immunol. 2021;12:702785. https://doi.org/10.3389/fimmu.2021.702785.
26. Sedighzadeh SS, Khoshbin AP, Razi S, Keshavarz-Fathi M, Rezaei N. A narrative review of tumor-associated macrophages in lung cancer: regulation of macrophage polarization and therapeutic implications. Transl Lung Cancer Res. 2021;10:1889–916. https://doi.org/10.21037/tlcr-20-1241.
27. Buck AK, et al. CXCR4-targeted theranostics in oncology. Eur J Nucl Med Mol Imaging. 2022;49:4133–44. https://doi.org/10.1007/s00259-022-05849-y.
28. Biasci D, et al. CXCR4 inhibition in human pancreatic and colorectal cancers induces an integrated immune response. Proc Natl Acad Sci U S A. 2020;117:28960–70. https://doi.org/10.1073/pnas.2013644117.
29. Hornburg M et al. Single-cell dissection of cellular components and interactions shaping the tumor immune phenotypes in ovarian cancer. *Cancer Cell* 39, 928–944.e926 (2021). https://doi.org/10.1016/j.ccell.2021.04.004
30. Qin R, et al. Role of chemokines in the crosstalk between tumor and tumor-associated macrophages. Clin Exp Med. 2023;23:1359–73. https://doi.org/10.1007/s10238-022-00888-z.
31. Dong L, et al. SPP1(+) TAM Regulates the Metastatic Colonization of CXCR4(+) Metastasis-Associated Tumor Cells by Remodeling the Lymph Node Microenvironment. Adv Sci (Weinh). 2024;11:e2400524. https://doi.org/10.1002/advs.202400524.
32. Lian SL, et al. Tumor-associated macrophages promoting PD-L1 expression in infiltrating B cells through the CXCL12/CXCR4 axis in human hepatocellular carcinoma. Am J Cancer Res. 2024;14:832–53. https://doi.org/10.62347/ziax8828.
33. Chew V, Toh HC, Abastado JP. Immune microenvironment in tumor progression: characteristics and challenges for therapy. *J Oncol* 2012, 608406 (2012). https://doi.org/10.1155/2012/608406
34. Xing S, Hu K, Wang Y. Tumor Immune Microenvironment and Immunotherapy in Non-Small Cell Lung Cancer: Update and New Challenges. Aging Dis. 2022;13:1615–32. https://doi.org/10.14336/ad.2022.0407.

35. Song J, et al. A Novel Ferroptosis-Related Biomarker Signature to Predict Overall Survival of Esophageal Squamous Cell Carcinoma. Front Mol Biosci. 2021;8:675193. https://doi.org/10.3389/fmolb.2021.675193.
36. Chen F, et al. Integrated Analysis of Cell Cycle-Related and Immunity-Related Biomarker Signatures to Improve the Prognosis Prediction of Lung Adenocarcinoma. Front Oncol. 2021;11:666826. https://doi.org/10.3389/fonc.2021.666826.
37. Geng R, et al. Crosstalk of Redox-Related Subtypes, Establishment of a Prognostic Model and Immune Responses in Endometrial Carcinoma. Cancers (Basel). 2022;14. https://doi.org/10.3390/cancers14143383.
38. Gu H, et al. Inflammation-Related LncRNAs Signature for Prognosis and Immune Response Evaluation in Uterine Corpus Endometrial Carcinoma. Front Oncol. 2022;12:923641. https://doi.org/10.3389/fonc.2022.923641.
39. Wu Y, et al. Spatiotemporal Immune Landscape of Colorectal Cancer Liver Metastasis at Single-Cell Level. Cancer Discov. 2022;12:134–53. https://doi.org/10.1158/2159-8290.Cd-21-0316.
40. Guo C, et al. Spatiotemporally deciphering the mysterious mechanism of persistent HPV-induced malignant transition and immune remodelling from HPV-infected normal cervix, precancer to cervical cancer: Integrating single-cell RNA-sequencing and spatial transcriptome. Clin Transl Med. 2023;13:e1219. https://doi.org/10.1002/ctm2.1219.
41. Song J, et al. Hypoxia inhibits ferritinophagy-mediated ferroptosis in esophageal squamous cell carcinoma via the USP2-NCOA4 axis. Oncogene. 2024;43:2000–14. https://doi.org/10.1038/s41388-024-03050-z.
42. Bischoff P, et al. Single-cell RNA sequencing reveals distinct tumor microenvironmental patterns in lung adenocarcinoma. Oncogene. 2021;40:6748–58. https://doi.org/10.1038/s41388-021-02054-3.
43. Zhu J, et al. Delineating the dynamic evolution from preneoplasia to invasive lung adenocarcinoma by integrating single-cell RNA sequencing and spatial transcriptomics. Exp Mol Med. 2022;54:2060–76. https://doi.org/10.1038/s12276-022-00896-9.
44. Sung H, et al. Global Cancer Statistics 2020: GLOBOCAN Estimates of Incidence and Mortality Worldwide for 36 Cancers in 185 Countries. CA Cancer J Clin. 2021;71:209–49. https://doi.org/10.3322/caac.21660.
45. Herbst RS, Morgensztern D, Boshoff C. The biology and management of non-small cell lung cancer. Nature. 2018;553:446–54. https://doi.org/10.1038/nature25183.
46. Gao S, et al. Neoadjuvant PD-1 inhibitor (Sintilimab) in NSCLC. J Thorac Oncol. 2020;15:816–26. https://doi.org/10.1016/j.jtho.2020.01.017.
47. Mandula JK, et al. Jagged2 targeting in lung cancer activates anti-tumor immunity via Notch-induced functional reprogramming of tumor-associated macrophages. Immunity. 2024;57:1124–e11401129. https://doi.org/10.1016/j.immuni.2024.03.020.
48. Dai X, et al. USP7 targeting modulates anti-tumor immune response by reprogramming Tumor-associated Macrophages in Lung Cancer. Theranostics. 2020;10:9332–47. https://doi.org/10.7150/thno.47137.
49. Wu J, Shen Y, Zeng G, Liang Y, Liao G. SPP1(+) TAM subpopulations in tumor microenvironment promote intravasation and metastasis of head and neck squamous cell carcinoma. Cancer Gene Ther. 2024;31:311–21. https://doi.org/10.1038/s41417-023-00704-0.
50. Pourbagheri-Sigaroodi A, Fallah F, Bashash D, Karimi A. Unleashing the potential of gene signatures as prognostic and predictive tools: A step closer to personalized medicine in hepatocellular carcinoma (HCC). Cell Biochem Funct. 2024;42:e3913. https://doi.org/10.1002/cbf.3913.
51. Smaldone G, et al. Targeting the CXCR4/CXCL12 Axis in Cancer Therapy: Analysis of Recent Advances in the Development of Potential Anticancer Agents. Molecules. 2025;30. https://doi.org/10.3390/molecules30061380.
52. Neves M, Marolda V, Mayor F, Jr., Penela P. Crosstalk between CXCR4/ACKR3 and EGFR Signaling in Breast Cancer Cells. Int J Mol Sci. 2022;23. https://doi.org/10.3390/ijms231911887.
53. Wu X, et al. CXCL12/CXCR4: An amazing challenge and opportunity in the fight against fibrosis. Ageing Res Rev. 2023;83:101809. https://doi.org/10.1016/j.arr.2022.101809.
54. Bianchi ME, Mezzapelle R. The Chemokine Receptor CXCR4 in Cell Proliferation and Tissue Regeneration. Front Immunol. 2020;11:2109. https://doi.org/10.3389/fimmu.2020.02109.


## Publisher's Note